JOURNAL OF SOLID STATE CHEMISTRY **130,** 35–41 (1997)
ARTICLE NO. SC967267

Synthesis, Crystal Structure, and Magnetic Properties of Sr_3MgMO_6 (M = Pt, Ir, Rh)

Pedro Núñez,[1] Steven Trail, and Hans-Conrad zur Loye[2]

Department of Chemistry, Massachusetts Institute of Technology, Cambridge, Massachusetts 02139

Received July 16, 1996; in revised form December 13, 1996; accepted December 19, 1996

The one-dimensional compounds Sr_3MgMO_6 (M = Pt, Ir, Rh) have been synthesized and structurally characterized by Rietveld refinement of powder X-ray diffraction data. All three compounds are isostructural with the rombohedral K_4CdCl_6-type structure (space group $R\bar{3}c$; $Z = 6$; Sr_3MgPtO_6: $a = 9.6481(5)$ Å, $c = 11.1169(7)$ Å; Sr_3MgIrO_6, $a = 9.6661(3)$ Å; $c = 11.1028$ Å; Sr_3MgRhO_6, $a = 9.6526(6)$ Å, $c = 11.0184(7)$ Å). The structure consists of infinite one-dimensional chains of alternating face-shared MO_6 octahedra (M = Pt, Ir, Rh) and MgO_6 trigonal prisms. The strontium cations are located in a distorted square antiprismatic environment. Magnetic susceptibility data show that both Sr_3MgIrO_6 and Sr_3MgRhO_6 obey the Curie–Weiss law with $\theta = -6(1)$ K, and $\theta = -15(3)$ K, respectively.

I. INTRODUCTION

The investigation of one-dimensional materials has been of interest to chemists and physicists because of their unique electronic and magnetic properties. The strong directionality of low-dimensional structures can produce highly anisotropic physical properties, since interactions between electrons, such as magnetic coupling, can be strongly dependent on the crystallographic directions along which they occur (1, 2). We recently reported the synthesis and characterization of several members of this family of materials including Sr_3ZnPtO_6 (3), Sr_3ZnIrO_6 (4), and $Sr_3CuPt_{0.5}Ir_{0.5}O_6$ (5), which exhibit magnetic behavior ranging from 1-D Ising to random quantum spin chain paramagnetism for Sr_3ZnIrO_6 and $Sr_3CuPt_{0.5}Ir_{0.5}O_6$, respectively. These one-dimensional compounds, as well as those described in this paper, are isostructural with Sr_4PtO_6 (6, 7), which has the K_4CdCl_6 structure type (8). The structure contains 1-D chains consisting of alternating face-sharing octahedra [MO_6] (M = Pt, Ir, Rh) and trigonal prisms [MgO_6]. Each chain is surrounded by six parallel neighboring chains that are separated by strontium cations, which are in a distorted square antiprismatic coordination.

Two papers reporting isostructural compounds, Sr_3CaRhO_6 (9) and Sr_3CaIrO_6 (10), have recently been published, and the relationship between the Sr_4PtO_6 structure type and that of the hexagonal perovskites was recently discussed (11). In this paper we report on the synthesis, magnetic properties, and structural characterization of the one-dimensional compounds, Sr_3MgPtO_6, Sr_3MgIrO_6, and Sr_3MgRhO_6.

II. EXPERIMENTAL

Sample Preparation

Polycrystalline samples of Sr_3MgMO_6 (M = Pt, Ir, Rh) were prepared by firing stoichiometric quantities of strontium carbonate (Alfa, 99.99%), magnesium acetate tetrahydrate (Alfa, 99.99%), and the corresponding powdered metal (Engelhard, 99.95%) in a platinum crucible overnight at 850°C to decompose the carbonate and acetate. Subsequently, the powders were ground and heated to 1050°C in alumina crucibles. Sr_3MgIrO_6 is almost completely formed after 1 day at 1050°C, although the reaction was allowed to proceed for a total of 4 days, with intermittent grinding. A final heating step at 1200°C for 12 h was added to improve the crystallinity of the sample. Sr_3MgPtO_6 was heated for 2 weeks at 1050°C and 4 days at 1150°C, with intermittent grinding. The same heating schedule was applied to Sr_3MgRhO_6; however, a significant amount of MgO impurity was observed by powder X-ray diffraction in the final product. For this reason the citrate method was used to synthesize the rhodium compound. Due to the insolubility of rhodium metal in acid, stoichiometric quantities of $SrCO_3$, $MgAc_2 \cdot 4H_2O$, and Rh metal grains were heated at 1150°C for 2 days. The resultant oxide mixture

[1] On leave at MIT. Permanent address: Departamento de Química Inorgánica, Universidad de La Laguna, E-38200 La Laguna, Tenerife (Spain).

[2] To whom all correspondence should be addressed at present address: Department of Chemistry and Biochemistry, University of South Carolina, Columbia, SC.

0022-4596/97 $25.00

was dissolved in nitric acid, and citric acid and ethylene glycol were added in a molar ratio of 1:2:2 (total metal:CA:EG). The pH was adjusted to 6.5 using ammonium hydroxide and the solution was concentrated by heating to about 80°C. Further heating to 200°C resulted in the formation of a black foam, which auto-ignited to form a fine powder. This powder was ground and heated at 800°C for several hours, followed by a heat treatment at 1000°C for 4 days with one intermittent grinding. Long heat treatment of these phases at high temperature led to the precipitation of magnesium oxide out of the material. A careful analysis of the powder X-ray diffraction data, described below, revealed that a very small MgO impurity is present in all three compounds. Sr_3MgPtO_6 is brownish-yellow in color; both Sr_3MgIrO_6 and Sr_3MgRhO_6 are black.

Crystal Structure

Powder X-ray diffraction data were collected on a Siemens D5000 powder diffractometer using Bragg–Brentano geometry with Cu$K\alpha$ radiation. The step scan covered the angular range 5°–118° in steps of 0.03° in 2θ. Three step scans were collected and summed. A detailed examination of the XRD patterns of Sr_3MgMO_6 (M = Pt, Ir, Rh) revealed a weak line at 43° (2θ), which cannot be indexed on the basis of the space group $R\bar{3}c$. This weak line was identified as the 100% peak of MgO.

Structure refinements of Sr_3MgMO_6 (M = Pt, Ir, Rh) were carried out in the space group $R\bar{3}C$ (No. 167), using the structure of Sr_4PtO_6 (6, 7) as the starting model (see Fig. 1). Based on our experience with the structurally related compounds Sr_3NiPtO_6 (12) and Sr_3ZnPtO_6 (3), the tetravalent metal was placed in the octahedral site 6*b*, the magnesium atom in the trigonal prismatic site 6*a*, and the strontium atom in the 18*e* site. Structure refinements were performed using the Rietveld method (13) implemented in the computer program FULLPROF (14). The profiles of the diffraction peaks were described by a standard pseudo-Voigt function varying two half-width parameters, U and W (refinement of V did not improve the fit and, therfore, V was set to zero and not refined) and the parameter η, which takes into account the Gaussian/Lorentzian contribution. Refinement of the peak asymmetry was performed using two additional parameters (15). The background was defined by a polynomial function with five refinable coefficients. One parameter was used for refinement of the zero point offset and one for the histogram scale factor.

Crystallographic data and further details of the Rietveld refinements are given in Table 1. The observed intensities, the calculated patterns, and their differences are shown in Fig. 2 for Sr_3MgPtO_6, in Fig. 3 for Sr_3MgIrO_6, and in Fig. 4 for Sr_3MgRhO_6. The atomic positions and the isotropic thermal parameters are listed in Table 2. Table 3 contains selected inter-atomic distances.

Bond valence calculations were carried out to check the structure of these phases; however, no parameters are available for Ir(IV) and Rh(IV). Using tabulated parameters (16), the following values were calculated for the estimated valence of the cations and the anions in each structure (17): Sr_3MgPtO_6, Sr (2.05), Mg (1.65), Pt (4.21), O (2.00),

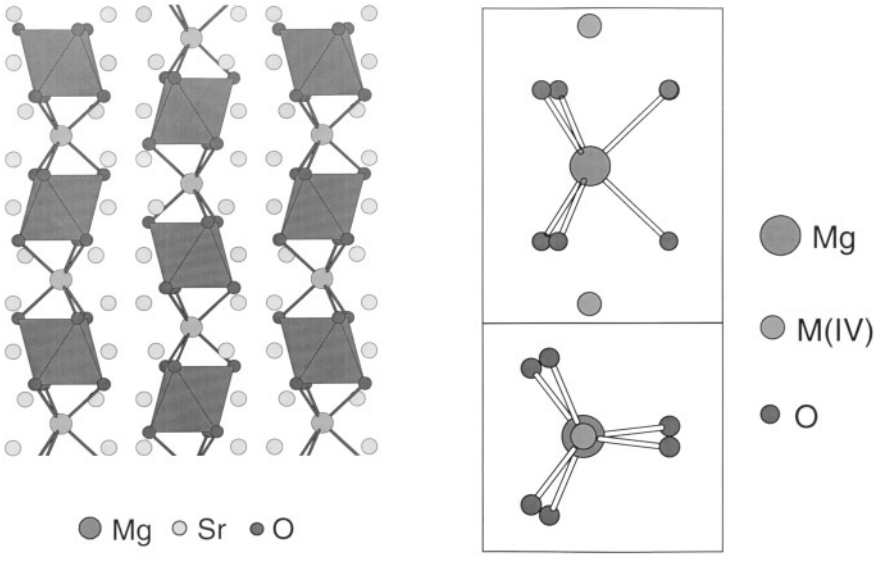

FIG. 1. The one-dimensional chain structure of $Sr_3MgM(IV)O_6$ (M(IV) = Pt, Ir, Rh) viewed along the **a**-axis is shown on the left. The [IrO_6] octahedra are shown as polyhedra, while all other atoms are shown in ball and stick format. The coordination environment around the trigonal prismatically coordinated magnesium is shown on the right.

TABLE 1
Summary of Crystallographic Data and Least-Squares Refinement Results for Sr_3MgMO_6 (M = Pt, Ir, Rh)[a]

Formula	Sr_3MgPtO_6	Sr_3MgIrO_6	Sr_3MgRhO_6
Space group	$R\bar{3}c$	$R\bar{3}c$	$R\bar{3}c$
a (Å)	9.6481 (5)	9.6661 (3)	9.6526 (6)
c (Å)	11.1169 (7)	11.1028(4)	11.0184(7)
No. of reflections	312	312	312
No. of refined parameters	22	22	22
No. of profile parameters	8	8	8
χ^2	4.51	3.14	4.03
R_B[b]	4.38	4.67	5.69
R_p[b]	7.61	6.52	7.13
R_{wp}[b]	9.88	8.48	9.21
R_{exp}[b]	4.65	4.78	4.59

[a] The e.s.d.'s have been corrected by a calculated factor {2.55 (Sr_3MgPtO_6), 2.46 (Sr_3MgIrO_6), and 2.58 (Sr_3MgRhO_6)} based on the method described by Berar Bérar *et al.* (23).

[b] See reference 24.

Sr_3MgIrO_6, Sr (2.09), Mg (1.53), O (1.99), and Sr_3MgRhO_6, Sr (2.10), Mg (1.67), O (2.02).

Magnetic Measurements

Magnetic susceptibilities of Sr_3MgIrO_6 and Sr_3MgRhO_6 were measured using a Quantum Design SQUID magnetometer in applied fields of 0.1, 0.5, and 4 T in the temperature range 5–305 K. The samples were zero field cooled and the magnetization was measured on heating. No significant differences were observed in the susceptibility vs temperature data collected in different applied fields. A correction was made for the clear gel capsules used as sample containers. No correction was made for the diamagnetic contribution of the non-paramagnetic species.

III. RESULTS AND DISCUSSION

Analysis of powder X-ray diffraction data indicates that the series of compounds Sr_3MgMO_6 (M = Pt, Ir, Rh) is isostructural with the rhombohedral K_4CdCl_6 structure type, as was expected based on the fairly large number of compounds that have been synthesized with this structure type. The differences in the radii of the 6-coordinate tetravalent cations (Pt^{+4} = 0.625 Å, Ir^{+4} = 0.625 Å, Rh^{+4} = 0.60 Å (18)) are noticeable in the slightly reduced **c** parameter for the Rh compound (11.0 vs. 11.1 Å). The Sr–O bond distances are in agreement with those found in analogous compounds (19). The Pt–O bond distances also are similar to those found in the literature (3, 12), similarly, for Rh–O (9) and for Ir–O (10). On the other hand, the size of the trigonal prismatic sites is sensitive to the size of cation hosted, as can be observed from the cell parameters (i.e., for Sr_4PtO_6, a = 9.74 Å; c = 11.90 Å (6)). Mg^{2+} has an ionic radius of 0.72 Å, which is rather small when compared to other cations that typically occupy this position in isostructural materials, Ca^{2+} = 1.00 Å, Sr^{2+} = 1.18 Å, or Ba^{2+} = 1.35 Å. The low value observed for the isotropic thermal factor (Table 2), as well as the estimated valence from bond valence calculations for Mg^{2+}, could be attributed to the inadequacy of the ionic size of magnesium relative to the trigonal prismatic site rather than to a cationic or anionic deficiency. This size inadequacy can also be used to rationalize the tendency of MgO to precipitate at higher synthesis temperatures in all three compositions investigated. This suggests

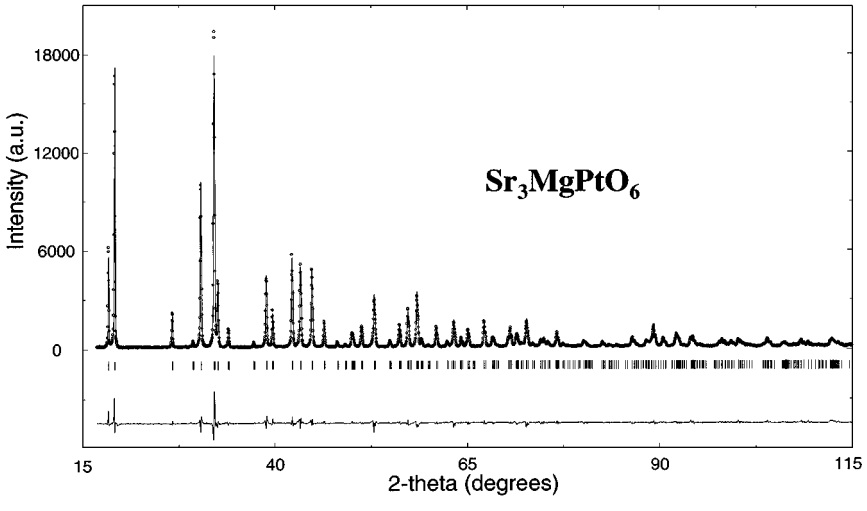

FIG. 2. Observed (circle) and calculated (solid line) X-ray profile of Sr_3MgPtO_6. Tick marks indicate the positions of allowed Bragg reflections. The difference line, observed minus calculated, is located at the bottom of the figure.

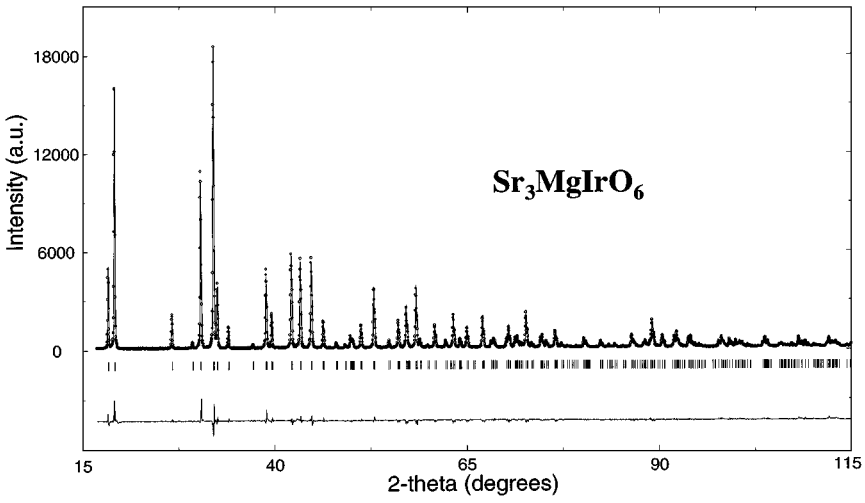

FIG. 3. Observed (circle) and calculated (solid line) X-ray profile of Sr_3MgIrO_6. Tick marks indicate the positions of allowed Bragg reflections. The difference line, observed minus calculated, is located at the bottom of the figure.

that these phases are not very thermally stable, since extended heat treatments also lead to the precipitation of MgO and emphasizes the need for low-temperature synthesis routes, such as the citric acid route used for the synthesis of Sr_3MgRhO_6.

Refinement of the phase fraction in all three compositions indicates that MgO is present as only a minor impurity phase, with a refined phase fraction of less than 1%. In the case of Sr_3MgRhO_6, the presence of MgO may also be the result of rhodium loss. This has been suggested for the analogous phases Sr_3CaRhO_6, where a small amount of rhodium was lost as a volatile oxide or incorporated in an amorphous impurity phase. By comparison, in our samples the impurity content was four times less than that found for Sr_3CaRhO_6 (9), and of the same order of magnitude as that found for Ca_4IrO_6 (10). In the Rietveld refinement, the most significant features in the difference profile are due to the inadequate peak shape function, rather than deficiencies in the structural model (Table 1).

The temperature dependence of the magnetic susceptibility of Sr_3MgIrO_6 and Sr_3MgRhO_6, measured at 5 kG, are shown in Figs. 5 and 6, respectively. The inverse susceptibilities vs temperature are also shown as inserts in Figs. 5 and 6. There are no significant differences between these data and those collected in 1 and 40 kG magnetic fields. All the magnetic measurements were made after zero field cooling of the samples. Table 4 summarizes the magnetic data for Sr_3MgIrO_6 and Sr_3MgRhO_6.

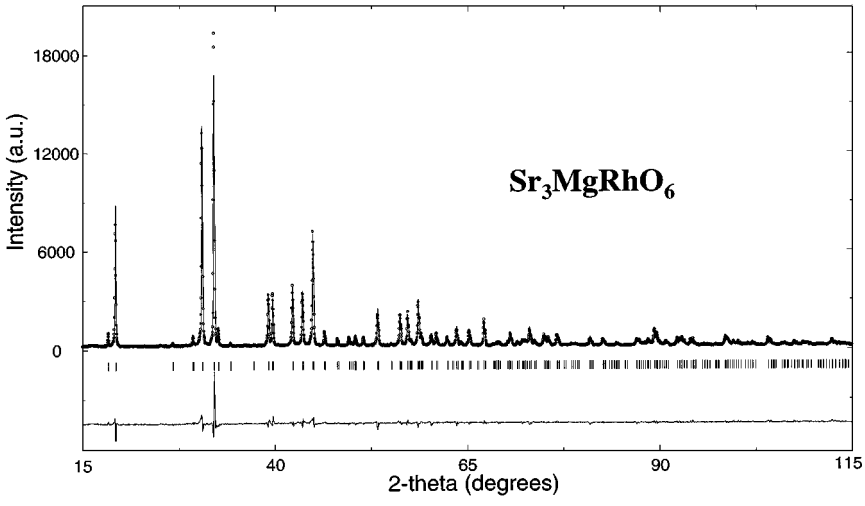

FIG. 4. Observed (circle) and calculated (solid line) X-ray profile of Sr_3MgRhO_6. Tick marks indicate the positions of allowed Bragg reflections. The difference line, observed minus calculated, is located at the bottom of the figure.

TABLE 2
Atomic Positions and Isotropic Thermal Parameters for Sr_3MgMO_6 (M = Pt, Ir, Rh)[a]

Compound	Atom	Site	x	y	z	B (Å^2)
Sr_3MgPtO_6	Sr	18*e*	0.3656(1)	0	1/4	1.46(8)
	Mg	6*a*	0	0	1/4	0.87(35)
	Pt	6*b*	0	0	0	1.26(7)
	O	36*f*	0.1721(16)	0.0 235(17)	0.1141(12)	1.76(38)
Sr_3MgIrO_6	Sr	18*e*	0.3644(3)	0	1/4	1.42(6)
	Mg	6*a*	0	0	1/4	1.45(31)
	Ir	6*b*	0	0	0	1.21(5)
	O	36*f*	0.1744(13)	0.0 234(13)	0.1126(10)	1.58(29)
Sr_3MgRhO_6	Sr	18*e*	0 .3656(3)	0	1/4	1.70 (8)
	Mg	6*a*	0	0	1/4	0 .56(33)
	Rh	6*b*	0	0	0	1.46(11)
	O	36*f*	0.1735(15)	0 .0 243(16)	0.1147(12)	1.50 (33)

[a] See footnote in Table 1.

The susceptibility vs temperature data of Sr_3MgIrO_6 was fitted to a Curie–Weiss law. No correction for the temperature independent paramagnetism (TIP) was made. For a low-spin d^5 ion (i.e., Ir(IV) or Rh(IV)) in a $t_{2g}^5 e_g^0$ electronic configuration the spin-only paramagnetic model predicts the following values: $S = 1/2$; $C = 0.375\ \text{emu} \cdot \text{K} \cdot \text{mol}^{-1}$; $\mu_{\text{eff}} = 1.73\ \mu_B$. The experimental Curie constant ($C = 0.277$) and the effective magnetic moment at room temperature ($\mu_{\text{eff}} = 1.40\ \mu_B$) obtained for Sr_3MgIrO_6 are smaller than those expected. However, these experimental values are in agreement with those obtained for analogous quaternary oxides (10). The negative value for the Weiss constant, $\theta = -6(1)$ K, and the maximum observed in Fig. 5 at 13 K indicate the presence of antiferromagnetic interactions.

The magnetic data for Sr_3MgRhO_6 were also fitted to a Curie-Weiss law, however, in this case temperature independent paramagnetism (TIP) was included as an important factor. The presence of TIP is clearly evidenced by the curvature of the high-temperature portion of the inverse magnetic susceptibility data shown in the inset of Fig. 6. The equation used for the fit was:

$$X_{\text{mol}} = C/(T - \theta) + \text{TIP}.$$

The estimated TIP contribution for Sr_3MgRhO_6 (300×10^{-6} emu $\cdot$ mol^{-1}) is slightly smaller than that reported for Sr_4RhO_6 (9) (540×10^{-6} emu $\cdot$ mol^{-1}). On the other hand, the TIP value assigned to Sr_3CaRhO_6 (10)

TABLE 3
Selected Interatomic Distances (Å) of Sr_3MgMO_6 (M = Pt, Ir, Rh)[a]

Compound	Bonds	Bond distances	Bonds	Bond distances
Sr_3MgPtO_6	Mg–O	2.172(16)	Mg–Sr	3.527(3)
	Pt–O	2.011(16)	Mg–Pt	2.779(1)
	Sr–O	2.498(17)–2.742(17)	Sr–Pt	3.209(3)
Sr_3MgIrO_6	Mg–O	2.200(13)	Mg–Sr	3.522(3)
	Ir–O	2.018(13)	Mg–Ir	2.776(1)
	Sr–O	2.484(13)–2.752(13)	Sr–Ir	3.219(1)
Sr_3MgRhO_6	Mg–O	2.166(14)	Mg–Sr	3.527(3)
	Rh–O	2.015(15)	Mg–Rh	2.755(1)
	Sr–O	2.481(15)–2.750(16)	Sr–Rh	3.208(1)

[a] See footnote in Table 1.

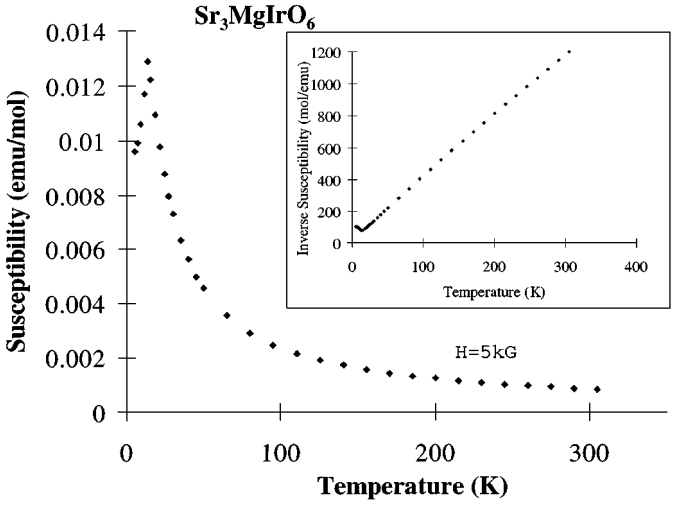

FIG. 5. Temperature dependence of the magnetic susceptibility of Sr_3MgIrO_6 measured at 5 kG. The inverse susceptibility vs temperature data are shown in the inset.

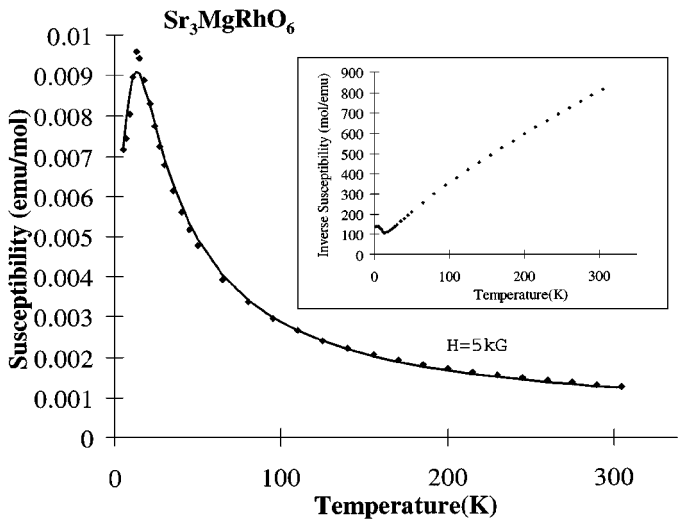

FIG. 6. Temperature dependence of the magnetic susceptibility of the Sr_3MgRhO_6 measured at 5 kG. The solid line represents the best fit to a 1-D Ising model (◆, experimental data). The inverse susceptibility vs temperature data are shown in the inset.

$(2850 \times 10^{-6}$ emu $\cdot$ mol$^{-1})$ is unusually high. In fact, the authors attribute the magnitude to an unidentified ferromagnetic impurity.

The experimental effective magnetic moment (1.73 μ_B) for Sr_3MgRhO_6 is in agreement with rhodium in a $+4$ oxidation state, eliminating the presence of the $+3$ oxidation state, since low spin d^6 Rh(III) is expected to be diamagnetic in an octahedral environment $t_{2g}^6 e_g^0$. We have obtained a Curie constant ($C = 0.287$ emu $\cdot$ K $\cdot$ mol^{-1}) that is smaller than the expected value for a paramagnetic spin-only system (see above). This low value can be explained in terms of short-range antiferromagnetic interactions, which increase at low temperature and are characterized by the Weiss constant ($\theta = -15(3)$K) and by the maximum in the magnetic susceptibility curve at ~ 13 K (Fig. 6).

TABLE 4
Magnetic Parameters for $Sr_3Mg\mathit{M}O_6$ (M = Ir, Rh)

	Sr_3MgIrO_6	Sr_3MgRhO_6
C (emu $\cdot$ K $\cdot$ mol^{-1})	0.252(2)	0.288(30)
θ (K)	−6(1)	−15(3)
TIP (emu $\cdot$ mol^{-1}) $\times 10^{+6}$	0	300
μ_{eff} (μ_B)[a]	1.41	1.73
J/k_B (K)[b]	−11	−14
g[b]	1.77	1.73
TIP[b] (emu $\cdot$ mol^{-1}) $\times 10^{+6}$	–	285

[a] $\mu_{eff} = (8 \cdot \chi \cdot T)^{1/2}$ μ_B where χ is the susceptibility molar (emu $\cdot$ mol^{-1}) at room temperature, T (K).

[b] Parameters determined by fitting an Ising model for a linear chain.

To explore the possible existence of low-dimensional magnetic ordering in these phases, the magnetic susceptibility data of Sr_3MgIrO_6 and Sr_3MgRhO_6 were also fitted to a one-dimensional Ising model (20). The parameters fitted were the intrachain exchange or interaction constant, J/k_B, and the average gyromagnetic ratio, g. In the case of Sr_3MgRhO_6, a TIP contribution was included in the equation as an additional constant term and refined as a third parameter. Table 4 lists the calculated values for J/k_B, g and TIP. The best fit to the Sr_3MgRhO_6 data is plotted as a solid line in Figure 6. The fit of the Ising model to the iridium compound data is not nearly as convincing as that to the rhodium compound data. While the fit to the data of Sr_3MgRhO_6 looks reasonable, this does not confirm the presence of low-dimensional magnetic behavior. The acute shape of the peak of the susceptibility can be related to the 1-D Ising model, but also to the Neel temperature of a three-dimensionally ordered system. Indeed, it will be necessary to carry out neutron diffraction and/or heat capacity measurements to confirm the 1-D Ising model.

In summary, we have prepared and characterized the compounds $Sr_3Mg\mathit{M}O_6$ (M = Pt, Ir, Rh), which crystallize with the $R\bar{3}c$ space group symmetry in the K_4CdCl_6 structure type. The $+4$ oxidation state for Pt, Ir, and Rh has been confirmed by the structural and magnetic data. The magnetic data for Sr_3MgIrO_6 and Sr_3MgRhO_6 obey a Curie–Weiss law with $\theta = -6(1)$ K and $\theta = -15(3)$ K, respectively.

This structure type is rather versatile and has led to the observation of a variety of interesting magnetic behavior. We succeeded in introducing a rather small cation (Mg^{+2}) into a large trigonal prismatic size. It is likely that additional isostructural materials can be made that will exhibit interesting magnetic behavior.

ACKNOWLEDGMENTS

This work was supported primarily by the MRSEC Program of the National Science Foundation under Award DMR:94-00334. P. N. thanks Dr. T. Roisnel (LLB, Saclay, France) for some help in the Rietveld refinement and DGICYT of Ministerio de Educación y Ciencia (Spain) for its financial support (Grant PR95-171).

REFERENCES

1. L. J. de Jongh and A. R. Miedema, *Adv. Phys.* **23,** 1 (1974).
2. P. Delhaes and M. Drillon (Eds.), "Organic and Inorganic Low Dimensional Crystalline Materials," NATO-ARW, Plenum, New York, 1987.
3. C. Lampe-Önnerud and H.-C. zur Loye, *Inorg. Chem.* **35,** 2155 (1996).
4. C. Lampe-Önnerud, M. Sigrist, and H.-C. zur Loye, submitted for publication.
5. T. N. Nguyen, P. A. Lee, and H.-C. zur Loye, *Science* **271,** 489 (1996).
6. J. J. Randall and L. Katz, *Acta Crystallogr.* **2,** 519 (1959).
7. I. Ben-Dor, J. T. Suss, and S. Cohen, *J. Crystal Growth* **64,** 395 (1983).
8. G. Bergerhoff and O. Schmitz-Dumont, *Z. Anorg. Allg. Chem.* **284,** 10 (1956).

9. J. F. Vente, J. K. Lear, and P. Battle, *J. Mater. Chem.* **5** (11), 1785 (1995)
10. N. Segal, J. F. Vente, T. S. Bush, and P. Battle, *J. Mater. Chem.* **6**(3), 395 (1996)
11. J. Darriet and M. Subramanian, *J. Mater. Chem.* **5,** 543 (1995).
12. T. N. Nguyen, D. M. Giaquinta, and H.-C. zur Loye, *Chem. Mater.* **6,** 1642 (1994).
13. H. M. Rietveld, *J. Appl. Crystallogr.* **2**, 65 (1969).
14. J. Rodriguez-Carvajal, "FULLPROF, ver.31c," LLB-CE, Saclay, France, 1996.
15. J. F. Bérar and G. Baldinozzi, *J. Appl. Crystallogr.* **26,** 128 (1993).
16. N. E. Bresse and M. O'Keeffe, *Acta Crystallogr. B* **47,** 192 (1991).
17. The bond valence values for the oxygen atoms in Sr_3MgIrO_6 and Sr_3MgRhO_6 are not very accurate. Each O atom is coordinated by 4 Sr atoms, one Mg atom and one tetravalent (Ir or Rh), and for the latter, the tabulated parameter for Pt(IV) was used instead of the true values for Ir(IV) or Rh(IV), which are not available.
18. R. D. Shannon, *Acta Crystallogr. A* **32,** 751 (1976)
19. See references 3, 9, 10, and 11 and references therein.
20. The Ising model for a spin system (21), in which only the z component of the spin angular moment interacts, is described by the Hamiltonian:

$$\mathbf{H} = -J \sum_{i,j} S_i^z S_j^z.$$

For the particular case of a one-dimensional system and spin $S = 1/2$, Fisher (22) has derived an equation for the parallel and perpendicular zero-field susceptibility. The averaged susceptibility is given by

$$\mathbf{X} = \frac{1}{3}\mathbf{X}_{//} + \frac{2}{3}\mathbf{X}_{\perp} = \frac{Ng^2\mu_B^2}{12J}\left[Ke^{-2K} + \tanh(K) + \frac{K}{\cosh^2(K)}\right],$$

where $K = |J/k_B T|$, g is the average gyromagnetic ratio, μ_B is the Bohr magneton, k_B is the Boltzman constant, and J is the exchange or interaction constant.

21. M. Ising, *Z. Phys.* **31,** 253 (1925).
22. M. E. Fisher, *J. Math. Phys.* **4,** 124 (1963).
23. J. F. Bérar and P. Lelann, *J. Applied Crystallogr.* **24,** 1 (1991).
24. Reliability factors were calculated as:

$$R_p = \sum_i |Y_{obs}^i - Y_{cal}^i| / \sum_i |Y_{obs}^i| \times 100$$

$$R_{wp} = \{\sum_i w_i |Y_{obs}^i - Y_{cal}^i|^2 / \sum_i w_i |Y_{obs}^i|\} \times 100$$

$$R_B = \sum_k |I_{obs}^k - I_{cal}^k| / \sum_k |I_k|$$

$$R_{exp} = \{[(N - P + C)/(\sum_i w_i |Y_{obs}^i|)]^{1/2}\} \times 100,$$

where Y_{obs}^i and Y_{cal}^i are observed and calculated intensity for the point i, respectively; and I_{obs}^k and I_{cal}^k are observed and calculated intensity for the reflections k, respectively. The weighted factor w_i was calculated as $w_i = 1/\sigma(Y_{obs}^i)$, where $\sigma(Y_{obs}^i)$ is the variance of the Y_{obs}^i. $N - P + C$ is the number of the degrees of freedom, where N equals the total number of points, P the number of refined parameters, and C the number of strict constraint functions. For a discussion on the reliability factors see reference (25).

25. E. Jansen, W. Schäfer, and G. Will, *J. Appl. Crystallogr.* **27,** 292 (1994)